

Evolution of Class II *TCP* genes in perianth bearing Piperales and their contribution to the bilateral calyx in *Aristolochia*

Natalia Pabón-Mora^{1,2} , Yesenia Madrigal¹ , Juan F. Alzate³ , Barbara A. Ambrose⁴ ,
Cristina Ferrándiz⁵ , Stefan Wanke², Christoph Neinhuis²  and Favio González⁶ 

¹Instituto de Biología, Universidad de Antioquia, Medellín 050010, Colombia; ²Technische Universität Dresden, Institut für Botanik, Dresden 01062, Germany; ³Facultad de Medicina, Universidad de Antioquia, Medellín 050010, Colombia; ⁴The New York Botanical Garden, Bronx, NY 10458, USA; ⁵Instituto de Biología Molecular y Celular de Plantas, Consejo Superior de Investigaciones Científicas – Universitat Politècnica de València, Valencia 46022, Spain; ⁶Facultad de Ciencias, Universidad Nacional de Colombia, Bogotá 111321, Colombia

Summary

Author for correspondence:
Natalia Pabón-Mora
Tel: +57 42195620
Email: lucia.pabon@udea.edu.co

Received: 14 March 2020
Accepted: 20 May 2020

New Phytologist (2020) **228**: 752–769
doi: 10.1111/nph.16719

Key words: *Aristolochia*, cell division, *CINCINNATA*, *CYCLOIDEA*, floral symmetry, Piperales.

- Controlled spatiotemporal cell division and expansion are responsible for floral bilateral symmetry. Genetic studies have pointed to class II *TCP* genes as major regulators of cell division and floral patterning in model core eudicots.
- Here we study their evolution in perianth-bearing Piperales and their expression in *Aristolochia*, a rare occurrence of bilateral perianth outside eudicots and monocots.
- The evolution of class II *TCP* genes reveals single-copy *CYCLOIDEA*-like genes and three paralogs of *CINCINNATA* (*CIN*) in early diverging angiosperms. All class II *TCP* genes have independently duplicated in *Aristolochia* subgenus *Siphisia*. Also *CIN2* genes duplicated before the diversification of *Saruma* and *Asarum*. Sequence analysis shows that *CIN1* and *CIN3* share motifs with Cyclin proteins and *CIN2* genes have lost the *miRNA319a* binding site.
- Expression analyses of all paralogs of class II *TCP* genes in *Aristolochia fimbriata* point to a role of *CYC* and *CIN* genes in maintaining differential perianth expansion during mid- and late flower developmental stages by promoting cell division in the distal and ventral portion of the limb. It is likely that class II *TCP* genes also contribute to cell division in the leaf, the gynoecium and the ovules in *A. fimbriata*.

Introduction

Bilateral floral symmetry has evolved multiple times independently during angiosperm diversification from the plesiomorphic radial condition (Citerne *et al.*, 2010). The result is a shift from actinomorphic (radially symmetric) flowers with several planes of symmetry to zygomorphic (dorsiventral or bilateral) flowers with one plane of symmetry (Leppik, 1972; Sargent 2004). Bilateral symmetry is established by differential cell division and cell expansion patterns that can result in organ elaboration, loss, displacement or fusion (Rudall & Bateman, 2004; Endress, 2012; Hileman, 2014). Thus, understanding the genetic basis underlying differences in cell division during development and growth of floral organs is essential to assess the repeated occurrence of bilateral symmetry across flowering plants.

Most independent acquisitions of bilateral symmetry have occurred in monocots and eudicots, with at least 23 transitions from actinomorphic to zygomorphic symmetry documented in the former and 46 in the latter (Citerne *et al.*, 2010). Bilateral symmetry before the diversification of monocots and eudicots is rare (Endress, 2012). In fact, the genus *Aristolochia* (Piperales), with *c.* 500 species, represents one of the few cases

of perianth bilateral symmetry in the magnoliids (Horn *et al.*, 2015). Although perianth plasticity across *Aristolochia* is extensive, the floral body plan in the genus is highly stable, resulting in a bilateral perianth shaped mainly by the differential curvature patterns between the adaxial and the abaxial portions of the perianth tube, and the monosymmetric perianth limb (González & Stevenson, 2000; Bliss *et al.*, 2013; Figs 1, 2). Developmental studies have shown that the perianth corresponds to three sepals undergoing early fusion and differential growth, which ends up in the typical convolute, often S- or U-shaped curvature (González & Stevenson, 2000; González & Pabón-Mora, 2015; Fig. 2). This floral body plan, probably acquired once before the diversification of the genus *Aristolochia*, strongly contrasts with the highly conserved radial perianth in all the remaining members of the perianth-bearing Piperales (*Asarum*, *Hydnora*, *Lactoris*, *Prosopanche*, *Saruma* and *Thottea*) (Figs 1, 2).

Class II *TCP* transcription factors *CYCLOIDEA* (*CYC*) and *DICHOTOMA* (*DICH*) are at the core of the genetic network responsible for flower bilateral symmetry. In the bilaterally symmetric flower of the model snapdragon (*Antirrhinum majus*, Plantaginaceae), *CYC* and *DICH* negatively control cell

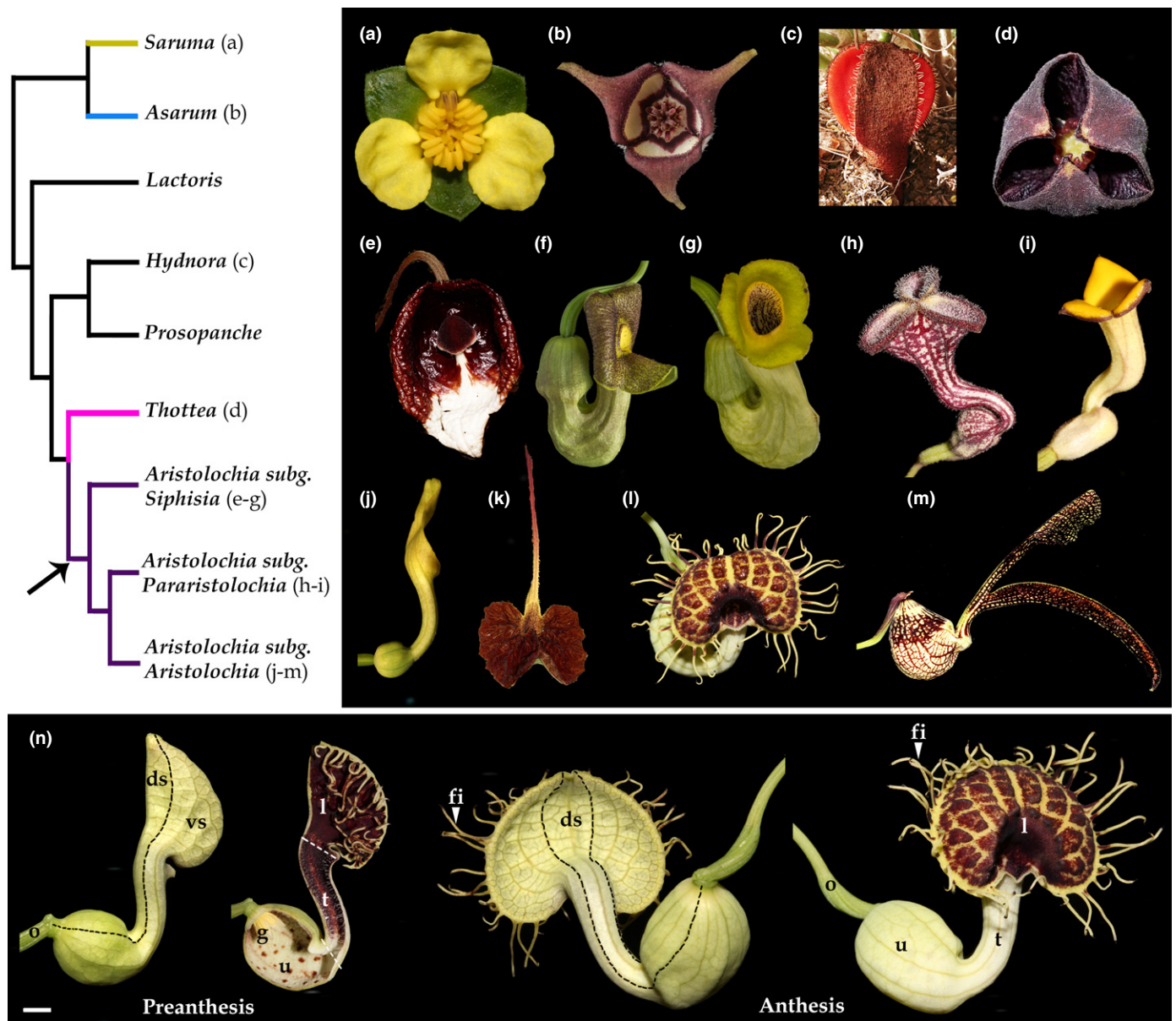


Fig. 1 Evolutionary shift from radially symmetric (a–d) to monosymmetric (e–m) perianth symmetry in the perianth-bearing Piperales (black arrow). (a) *Saruma henryi* (yellow branch); (b) *Asarum canadense* (blue branch); (c) *Hydnora africana*; (d) *Thottea siliquosa* (pink branch). (e–g) Members of *Aristolochia* subgenus *Siphisia*: (e) *A. arborea*; (f) *A. macrophylla*; (g) *A. manshuriensis*. (h, i) Members of *Aristolochia* subgenus *Pararistolochia*: (h) *A. deltantha*; (i) *A. praevenosa*. (j–m) Members of *Aristolochia* subgenus *Aristolochia*: (j) *A. clematidis*; (k) *A. lindneri*; (l) *A. fimbriata*; (m) *A. ringens*. (n) *Aristolochia fimbriata* flowers in preanthesis and anthesis showing dorsal and ventral portions of the perianth and utricle, tube and limb. The purple subclade indicates members of *Aristolochia*; ds, dorsal perianth portion; fi, fimbriae; g, gynostemium; l, limb; o, ovary; t, tube; u, utricle; vs, ventral perianth portion. Bar, 0.5 cm.

proliferation in the dorsal portions of the flower, as shown by the ventralized radial flowers of *cycl/dich* mutants (Luo *et al.*, 1996, 1999; Martín-Trillo & Cubas, 2010). *CYC* and *DICH* positively regulate *RADIALIS* (*RAD*), a *MYB* transcription factor known to limit cell division in the dorsal sector of the flower (Corley *et al.*, 2005). *RAD* also outcompetes its *MYB* homolog *DIV* in the dorsal sector of the flower, limiting *DIV* function to the ventral and lateral petals (Almeida *et al.*, 1997; Galego & Almeida, 2002). *DIV* remains in charge of establishing ventral differentiation, as shown by the *div* mutant flowers in which the ventral petal

becomes similar to the lateral petals (Almeida *et al.*, 1997; Galego & Almeida, 2002).

The use of the snapdragon genetic model as a reference point for other flowering plants exhibiting bilateral symmetry is influenced by the evolutionary history of the gene lineages themselves and, to an extent, is limited by the scarce functional studies across homologs in different plant lineages. Both the *MYB* and the *TCP* genes have undergone reiterative duplication events resulting in very divergent genetic complements across flowering plants. For instance, within *TCP* transcription factors, *CYC* genes have

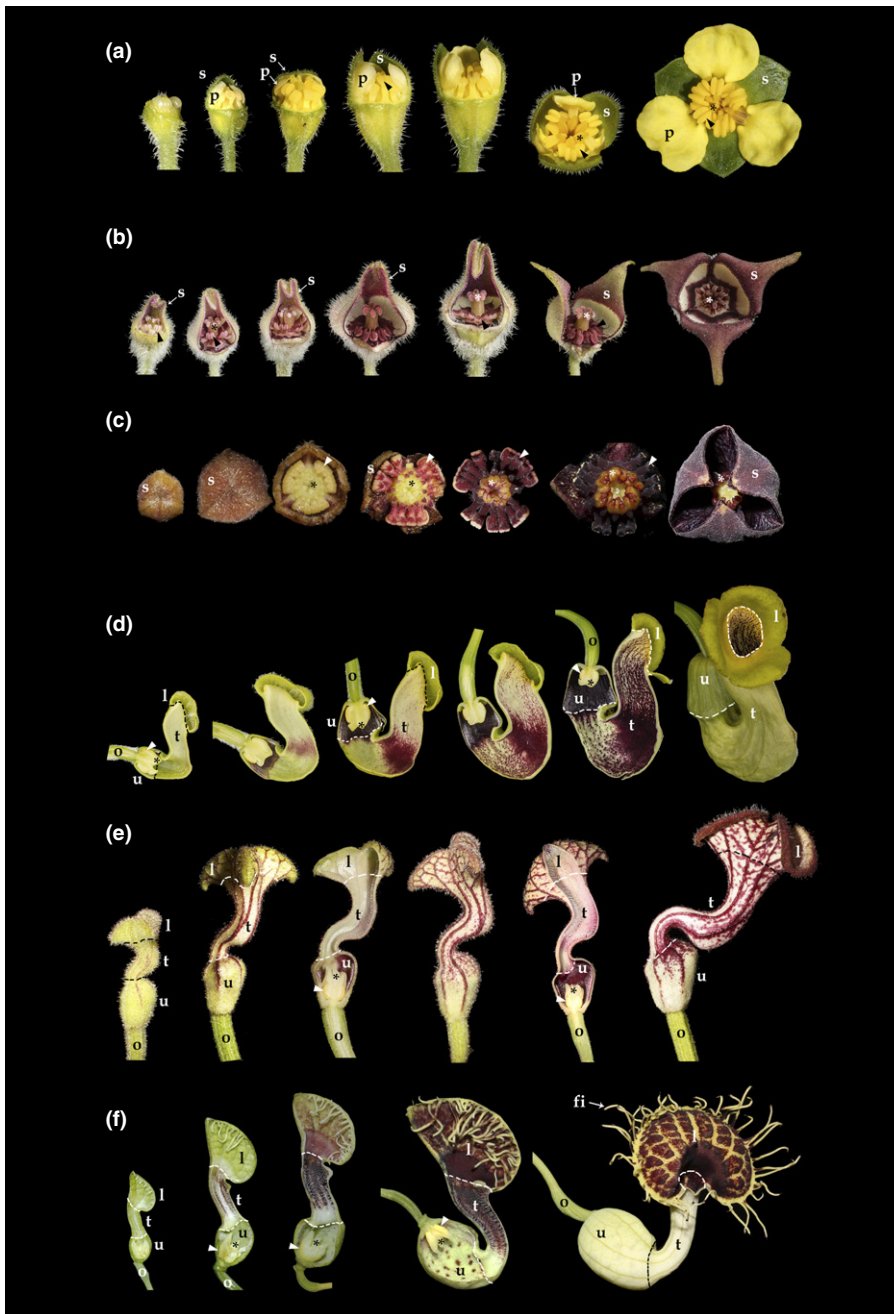


Fig. 2 Mid-to-late floral stage of: (a) *Saruma henryi*, (b) *Asarum canadense*, (c) *Thottea siliquosa*, (d) *Aristolochia* (subgenus *Siphisia*) *manshuriensis*, (e) *A.* (subgenus *Pararistolochia*) *deltantha*, (f) *A.* (subgenus *Aristolochia*) *fimbriata*. Arrowheads point to stamens; asterisks point to stigmatic lobes; broken lines in (d), (e) and (f) indicate the utricle/tube/limb portions; l, limb; o, ovary; p, petal; s, sepal; t, tube; u, utricle (see Pabón-Mora *et al.*, 2015 for details).

undergone two duplications in core eudicots, resulting in the *CYC1*, *CYC2* and *CYC3* clades (Cubas *et al.*, 1999; Howarth & Donoghue, 2006; Martin-Trillo & Cubas, 2010). Specifically, *CYC* and *DICH* are *CYC2* paralogs found in *Antirrhinum* as a result of a Plantaginaceae-specific whole-genome duplication (Li *et al.*, 2019). Expression and functional data corroborate that *CYC2* genes have been independently recruited to establish floral bilateral symmetry not only in the Plantaginaceae, but also in members of the Asterales, Brassicales, Dispacales, Fabales and Malpighiales, among others (Busch & Zachgo, 2007; Preston *et al.*, 2009; Wang *et al.*, 2010; Zhang *et al.*, 2010, 2013; Howarth *et al.*, 2011; Elomaa *et al.*, 2018). Moreover, *CYC-like* genes present in noncore eudicots appear to have duplicated independently

several times in monocots and early diverging eudicots (Mondragón-Palomino & Trontin, 2011; Madrigal *et al.*, 2017). In some instances, they have also been recruited independently for the establishment of bilateral symmetry; this appears to be the case in Papaveraceae and Proteaceae (Damerval *et al.*, 2007, 2017, 2019; Citerne *et al.*, 2016), as well as in a few monocots including Commelinaceae and Zingiberaceae (Bartlett & Specht, 2011; Preston & Hileman, 2012). Nevertheless, expression analyses by *in situ* hybridization of the preduplicated *CYC-like* genes in *Aristolochia arborea* (*AarCYC*) show low and homogenous expression in the perianth (Horn *et al.*, 2015). Here, no differences in expression of the *AarCYC* genes are detected in the dorsal versus the ventral sides of the perianth. In addition,

heterologous functional studies overexpressing *AarCYC* genes in *Arabidopsis* further suggested that they are not responsible for the establishment of bilateral perianth symmetry, at least in this species (Horn *et al.*, 2015).

Whether other class II *TCP* transcription factors could promote the establishment or maintenance of bilateral symmetry in *Aristolochia* is still unknown. A recent study attempting to identify differentially expressed genes (DEGs) in the utricle, the tube and the limb of the *Aristolochia ringens* perianth, recovered three class II *TCP*, *CINCINNATA* genes in all three-way comparisons among the top 20 DEGs (Suárez-Baron *et al.*, 2019). These results suggested important roles of *CIN* in shaping the proximal-distal specializations in the *Aristolochia* perianth. However, as the focus of the study in *A. ringens* was not directed towards floral symmetry candidate genes, the results cannot be directly compared with the available data on *A. arborea* (Horn *et al.*, 2015). In turn, it is as yet unclear whether any of the class II *TCP* genes contribute to perianth bilateral symmetry in other species of *Aristolochia*. Here we aim to assess the evolution of class II *TCP* genes across the perianth-bearing Piperales in order to determine how copy number and protein sequence have changed in the group (Fig. 1). In addition, we aim to establish the expression patterns of *CYC* and *CIN* genes in *Aristolochia fimbriata* in order to investigate whether these transcription factors have an effect on the establishment and maintenance of the bilateral symmetry and the patterning of the perianth during development and differential growth. *Aristolochia fimbriata* was selected for the spatio-temporal *in situ* hybridization expression analyses, as it is a small-sized plant, easy to grow in laboratory settings, and flowers profusely. In addition, it has a reference transcriptome from mixed leaves, flowers and fruits and has extensive preliminary data on the expression of other transcription factors establishing the identity of floral organs (Bliss *et al.*, 2013; Pabón-Mora *et al.*, 2015; Suárez-Baron *et al.*, 2016; Pérez-Mesa *et al.*, 2020). Hence, it has become a representative species of the genus *Aristolochia* for evolutionary developmental biology studies.

Materials and Methods

Reference RNA-seq for perianth-bearing Piperales

Reference transcriptomes were generated *de novo* from seven species across all three subgenera of *Aristolochia*, two from subgenus *Aristolochia* (*A. clematitis* L. and *A. lindneri* A. Berger), two from subgenus *Pararistolochia* (*A. deltantha* F. Muell., and *A. praevenosa* F. Muell.) and three from subgenus *Siphisia* (*A. arborea* Linden., *A. macrophylla* Lam. and *A. manshuriensis* Kom.). Two additional transcriptomes from *A. fimbriata* and *A. ringens* (both members of subgenus *Aristolochia*), previously available (Pabón-Mora *et al.*, 2015; Suárez-Baron *et al.*, 2019), were also included in the present study. Four additional transcriptomes from *Asarum* (*A. canadense* L. and *A. europaeum* L.), *Saruma* (*S. henryi* Oliv.) and *Thottea* (*T. siliquosa* (Lam) Ding Hou) were generated *de novo*. In general, all available above-ground organs were collected, including young leaves, flowers at different stages of development (Fig. 2) and young fruits when

available. All organs and tissues were mixed for RNA extraction as the goal was to have a reference mixed transcriptome to isolate as many expressed class II *TCP* genes as possible. The material was gathered from the living collections of the Arnold Arboretum at Harvard University (Roslinale, MA, USA), the Botanical Garden of the University of Technology Dresden (Dresden, Germany) and the Botanical Garden of Medellín (Medellín, Colombia; Supporting Information Table S1). Tissue was flash-frozen in liquid nitrogen and stored at -80°C until further processing. Total RNA from each species was extracted using TRIzol reagent (Invitrogen) or TRIsure (Meridian Life Science Inc., Memphis, TN, USA), resuspended in 1 ml of 100% ethanol and sent to the sequencing facility. The RNAseq experiment was conducted using the Truseq mRNA library construction kit (Illumina) and sequenced on a HiSeq2000 instrument reading 100 bases, paired-end reads. Read cleaning was performed with a quality threshold of Q30 and a minimum read length of 70 bases. Contig assembly was computed using the TRINITY package following default settings and TRIMMOMATIC flag. Standard metrics for each transcriptome were calculated (Table S1).

Gene homolog searches and phylogenetic analyses

In order to isolate putative *CYC* and *CIN* homologs in our generated transcriptomes, previously reported sequences from selected angiosperms were used as queries (Horn *et al.*, 2015; Madrigal *et al.*, 2017; Suárez-Baron *et al.*, 2019). Searches were done using TBLASTX tools (Altschul *et al.*, 1990) on all transcriptomes newly assembled in this work (Table S1) and those available from previous studies from *A. fimbriata* and *A. ringens* (Pabón-Mora *et al.*, 2015; Suárez-Baron *et al.*, 2019). All sequences isolated were compiled with BIOEDIT (<http://www.mbio.ncsu.edu/BioEdit/bioedit.html>). Two independent phylogenetic analyses were done. A first comprehensive analysis included previously published class II *TCP* genes from across angiosperms (Horn *et al.*, 2015; Citerne *et al.*, 2016; Madrigal *et al.*, 2017; Damerval *et al.*, 2019; Fig. S1). A second focused analysis only included the reference canonical genes from *Arabidopsis*, *Antirrhinum* and the newly isolated homologs from the perianth-bearing Piperales (Fig. 3). Nucleotide sequences were aligned using the online version of MAFFT (<http://mafft.cbrc.jp/alignment/software/>) (Katoh *et al.*, 2002) with a gap open penalty of 4.0, offset value of 1.0 and all other default settings. The alignments were then refined manually using BIOEDIT considering as a reference the 60–70 amino acids reported as conserved in the TCP protein domain (Cubas *et al.*, 1999). Phylogenetic analyses of the *CYC/CIN* gene lineages were performed using maximum likelihood (ML) with IQ-TREE (Nguyen *et al.*, 2015). The evolution model that best fit our data was selected with MODELFINDER integrated in IQ-TREE (Kalyaanamoorthy *et al.*, 2017). Supports were estimated using the UltraFast Bootstrap (UFB) method using 1000 pseudoreplicates (Hoang *et al.*, 2018). RAXML phylogenetic analyses were also generated with the same data for comparison, through the CIPRES portal (Miller *et al.*, 2010). The *Amborella trichopoda* PCF-like sequence (*AmtrTCP4*) was used as outgroup in both analyses. The tree was observed and edited using FIGTREE v.1.4.3

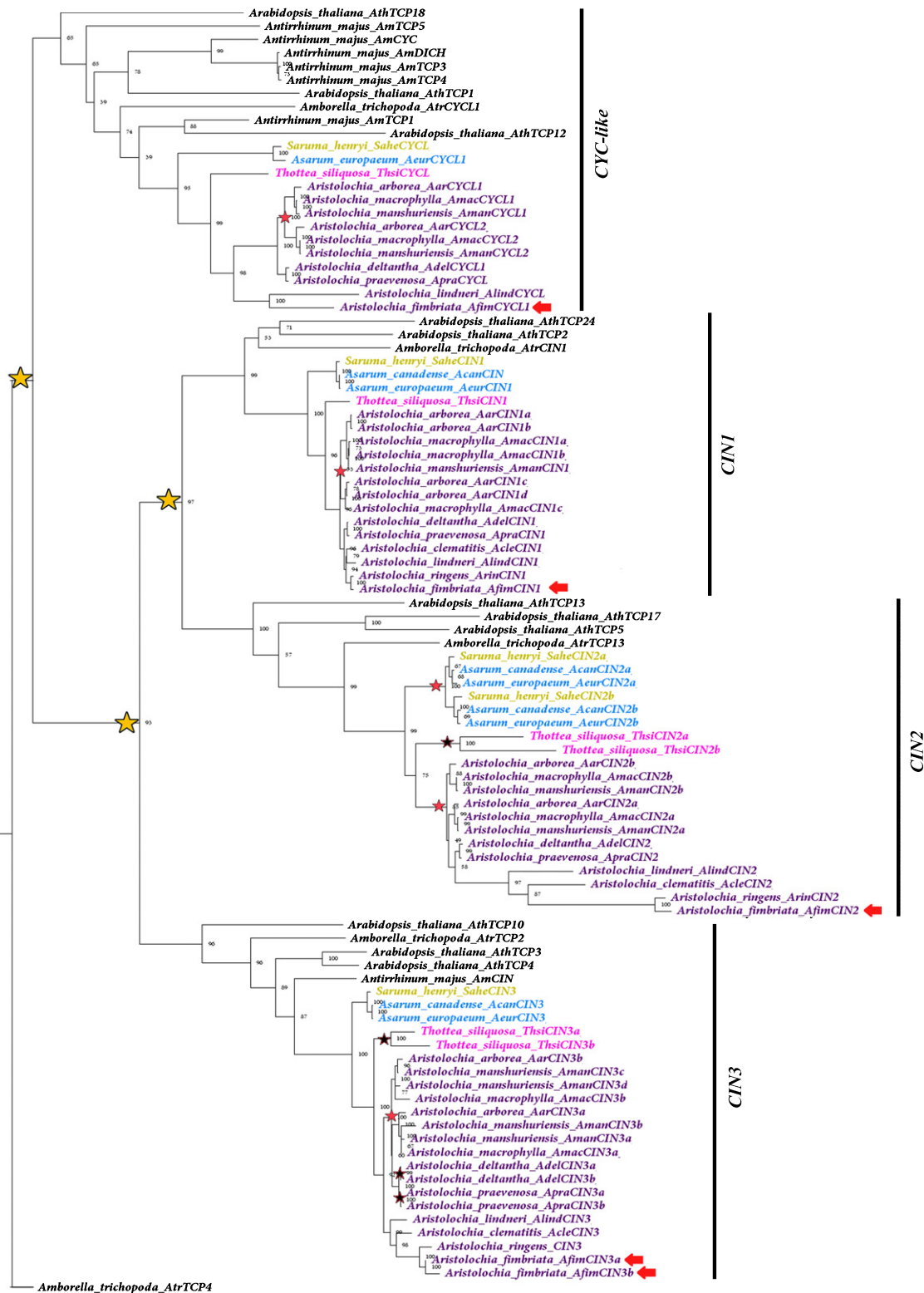


Fig. 3 Phylogenetic analysis of the class II TCP genes with an expanded sampling in Aristolochiaceae using the *Amborella trichopoda* TCP4 PCF gene as outgroup. As reference for homology the canonical *Antirrhinum majus*, *Arabidopsis thaliana* and homologs from *Amborella trichopoda* (black names) were also included. Homologs of *Saruma henryi* in yellow, homologs of *Asarum* in blue, homologs of *Thottea siliquosa* in pink, homologs of *Aristolochia* in purple. Yellow stars indicate large-scale duplications occurring before the diversification of angiosperms; red stars indicate local clade-specific duplications in Aristolochiaceae; black stars indicate species-specific duplications; red arrows point to the *Aristolochia fimbriata* homologs. CYC-like, CYCLOIDEA-LIKE genes; CIN1, CIN2, CIN3, CINCINNATA 1, 2 and 3.

(Rambaut, 2014). The new isolated sequences from our transcriptomes were deposited in the GenBank under the numbers MN786975–MN787024 and MT136782–MT136801.

Identification of protein motifs in canonical class II TCP genes and the perianth-bearing Piperales homologs

In order to detect reported as well as new conserved motifs, all sequences were permanently translated, uploaded as amino acids to the online Multiple Em for Motif Elicitation (MEME) server (<http://meme.nbcr.net>) and run with all the default options. The motifs retrieved by MEME are reported according to their statistical significance. Within the given sequences, the MEME suite finds the most statistically significant (low e-value) motifs first. We did the search for 15 motifs arbitrarily to search beyond the noncanonical basic helix–loop–helix (bHLH) large domain characteristic of all TCP proteins. The e-value of a motif is based on its log likelihood ratio, width, sites, and the size of the set.

RT-PCR expression analyses

To examine and compare the expression patterns of class II TCP genes and assess their contribution to differential dorsiventral differentiation during flower development, we dissected the dorsal and the ventral portions of the *A. fimbriata* perianth from stages S6 to S8 (stages following Pabón-Mora *et al.*, 2015). All other floral parts were removed. Total RNA was isolated from each floral region using TRIzol (Invitrogen) following the manufacturer's protocol and resuspended in 20 µl of DEPC water. RNA was treated with RQ DNaseI RNase-free (Promega, Madison, WI, USA) to remove genomic DNA contamination. RNA was quantified with a Nanodrop 2000 spectrophotometer (Thermo Scientific, Waltham, MA, USA). The cDNA was synthesized using 3 µg of total RNA as template and oligo-dT primers to select for mRNA. Primers were designed in specific regions outside the bHLH domain for each copy (Table S2). Each amplification reaction incorporated EconoTaq (Lucigen, Middleton, WI, USA), nuclease-free water, BSA, Betaine, forward and reverse primers (10 mM each) and 1 µl of undiluted cDNA for a 20 µl total reaction. Thermal cycling profiles included an initial denaturation step (94°C for 3 min) followed by 30–35 cycles of denaturation (94°C for 30 s), annealing (55°C for 33 s) and extension (72°C for 40 s). *ACTIN* was used as a positive control. The PCR products were visualized in a 1.5% agarose gel stained with ethidium bromide and digitally photographed using a BioDoc Analyzer (Biometra, Jena, Germany).

In situ hybridization expression analyses

Vegetative apices, inflorescences, floral buds and fruits of *A. fimbriata* at several developmental stages were collected and fixed in formaldehyde–acetic acid–ethanol (3.7% formaldehyde : 5% glacial acetic acid : 50% ethanol). The material was dehydrated through an alcohol-histochoice series and embedded in Paraplast X-tra (Fisher Healthcare, Houston, TX, USA). Samples embedded were maintained at 4°C until use. Samples were sectioned

with a rotary microtome (Microm HM3555; Microm International GmbH, Thermo Fisher Scientific, Walldorf, Germany) at 8–10 µm. DNA templates for RNA probe synthesis were obtained by PCR amplification of fragments between 120 and 600 bp for all genes except *AfimCIN2*. The reasons for excluding *AfimCIN2* from *in situ* hybridization analyses are that: *AfimCIN2* lacks expression in early developmental stages (S0–S5); and it has more homogeneous expression in the dorsal and ventral portions of the perianth in mid- and late floral developmental stages, showing only faint bands after 35 amplification cycles in reverse transcription polymerase chain reaction (RT-PCR) (see the Results section; Fig. S3). To ensure specificity, the probe templates were designed flanking the bHLH domain in positions where sequences varied between the TCP paralogs: *AfimCYC* (590 bp probe size), *AfimCIN1* (335 bp probe size) and *AfimCIN3a* (318 bp probe size). The only exception was *AfimCIN3b* (128 bp probe size) whose probe was designed in the 5' upstream the bHLH domain where it presented differences with *AfimCIN3a*. *HISTONE4* was used to detect cell division in all organs during all developmental stages included in the hybridizations (Table S2).

Gene-specific probe fragments were amplified with Takara Taq (TaKaRa, Saint-Germain-en-Laye, France), nuclease-free water, BSA (5 µg ml⁻¹), Q solution (5 µg µl⁻¹), forward and reverse primers (10 mM each), and 1 µl of template cDNA for a total of 20 µl. Thermal cycling profiles followed an initial denaturation step (94°C for 30 s), an annealing step (50–59°C for 30 s) and an extension step (72°C for 1 min) for 30–38 amplification cycles. DNA PCR fragments were cleaned using the QIAquick PCR purification Kit (Qiagen). Digoxigenin-labeled RNA probes were prepared using T7 RNA polymerase (Roche), RNase inhibitor RNasin (New England Biolabs, Ipswich, MA, USA) and RNA labeling mix (Roche, Switzerland) according to the manufacturer's protocol. RNA *in situ* hybridization was performed following Ambrose *et al.* (2000) and Ferrándiz *et al.* (2000). *In situ* hybridized sections were subsequently dehydrated and permanently mounted in Permount (Fisher, Waltham, MA, USA). All sections were digitally photographed using a Zeiss Axioplan microscope equipped with a Nikon DXM1200C digital camera.

Results

The *Aristolochia* perianth is the result of early fusion and curvature of three sepals

Careful floral dissections were done in *Saruma henryi*, two species of *Asarum*, *A. canadense* and *A. europaeum*, and *Thottea siliquosa* (Fig. 2). These three genera were used as representative perianth-bearing Piperales with radial floral symmetry. *Saruma henryi* is the only member with a bipartite (with calyx and corolla) perianth, which contrasts with the unipartite, sepal-derived perianth in *Asarum* and *Thottea* (González & Stevenson, 2000; González & Pabón-Mora, 2015). Within *Aristolochia*, representative species from all three subgenera were imaged in detail. *Aristolochia manshuriensis* as a representative of subgenus *Siphisia*,

A. deltantha as a representative of subgenus *Pararistolochia*, and our target species in this study, *A. fimbriata*, as a representative of subgenus *Aristolochia*. In all *Aristolochia* species, the perianth is the result of early fusion of three sepals (González & Stevenson, 2000), which grow together and differentiate into a proximal, inflated utricle, followed by a tube and ending into a distal, expanded limb. The utricle/tube juncture is probably the perianth region that curves the most during floral growth. The stamens and the stigmatic lobes are also fused into a structure called the gynostemium (Pérez-Mesa *et al.*, 2020). Unlike the perianth, the gynostemium is radially symmetric. The ovary is inferior and its distal portion is connected with the style and the stigmatic lobes through a common compitum. While the three calyx lobes can be easily distinguished in all members of the subgenus *Siphisia*, including *A. macrophylla* and *A. manshuriensis*, as well as in all members of subgenus *Pararistolochia*, including *A. deltantha* and *A. praevenosa*, they cannot be readily identified in the members of subgenus *Aristolochia*, including *A. clematitidis*, *A. fimbriata*, *A. lindneri* and *A. ringens* (Figs 1, 2).

Evolution of the class II TCP transcription factors

In order to establish the homology of the class II TCP genes isolated from selected members of the Aristolochiaceae, two different analyses were done. The first one included the 75 sequences isolated by BLAST from our transcriptomes into a comprehensive matrix, including most class II TCP genes from Horn *et al.* (2015), Citerne *et al.* (2016), Madrigal *et al.* (2017), and Damerival *et al.* (2019), for a total of 255 sequences and 3634 characters (Fig. S1). The second one was restricted to the newly isolated sequences and the canonical class II TCP genes from *Arabidopsis thaliana* (10) and *A. majus* (seven), plus four *Amborella trichopoda* hits for a total of 96 sequences and 2487 characters. Both analyses recovered the *CYC*, *CIN1*, 2 and 3 clades, resulting from duplication events predating angiosperm diversification (Figs S1, 3). So far, class II TCP gene sampling has been heavily concentrated towards *CYC* genes compared with *CIN* genes (Fig. S1). Thus, we will focus on the results of the second analyses where equally representative sampling from all clades is shown. In the *CYC-like* clade (UFB = 65) core eudicot copies are recovered from the *A. majus* and *A. thaliana* canonical sequences. *CYC-like* homologs in the Aristolochiaceae are retained in most species as single copy, except for the species belonging to *Aristolochia* subgenus *Siphisia*, which have two *CYC-like* copies as a result of a local duplication event (Fig. 3). By comparison, the *CIN* clade (UFB = 93) shows two rounds of duplication events before angiosperm diversification, resulting in three clades, namely *CIN1* (UFB = 99), *CIN2* (UFB = 100) and *CIN3* (UFB = 96). At least one of these duplications has been previously reported by Madrigal *et al.* (2017); however, we have renamed all clades according to the current results (Fig. 3). Thus, Madrigal *et al.*'s (2017) *CIN1* clade is split here into *CIN1* and *CIN2*; in addition, Madrigal *et al.*'s (2017) *CIN2* clade corresponds to *CIN3* in this study. Additional duplications have occurred in each of the gene clades described so far. The duplications in the *CIN1* and *CIN3* clades predate the diversification of

subgenus *Siphisia*, as seen by the two copies found in *A. arborea*, *A. macrophylla* and *A. manshuriensis*. Within the clade *CIN2*, the analysis recovers two additional duplications, one before the diversification of *Asarum* and *Saruma* and a second one before the diversification of *Aristolochia*. After this second duplication, the two *CIN2* copies were only retained in subgenus *Siphisia* and lost in the remaining two subgenera of *Aristolochia*. Species-specific duplications were detected for *CIN2* in *Thottea siliquosa*, with two copies, and for *CIN3* in the members of subgenus *Pararistolochia* examined (*A. deltantha* and *A. praevenosa*), both with two copies. All *CIN* orthologs appear as single-copy genes in all examined species of subgenus *Aristolochia* (*A. clematitidis*, *A. fimbriata*, *A. lindneri* and *A. ringens*) with the exception of *CIN3* in *A. fimbriata*, where two contigs were identified. These could correspond to two copies or two alternative splicing forms (Fig. 3).

Protein domains and motifs identified in the class II TCP transcription factors isolated

The MEME analysis allowed us to map the bHLH domain characteristic to all TCP genes in motifs 1 and 3 (Figs S2, S3). The beginning of helix II in the bHLH domain, here contained at the end of motif 1, was inspected in detail to compare the canonical amino acids reported to be key for protein interactions. TCP proteins of *Antirrhinum* and *Arabidopsis* were compared with the TCP proteins isolated from Aristolochiaceae and *Amborella*. Changes are observed between the core eudicot LxxLL motif and the early angiosperm VxxLL motif in *CYC* proteins. Conversely, no changes are detected between the core eudicot *CIN1* (VEWLI) and *CIN3* (VDWLI) motifs in this region and their early divergent angiosperm homologs and only the first position in the xDWLL motif in *CIN2* proteins varies within core eudicot copies sampled (Fig. 4). The *CIN1* (VEWLI) and *CIN3* (VDWLI) motifs are also present in Cyclin proteins. Most *CYC* proteins have an R-domain putatively mediating protein–protein interactions, downstream of the bHLH, which was found through manual inspection with notable variations and thus not recovered in the MEME analyses. The same R motif is found in *CIN1* proteins in motif 6 and is lacking from *CIN2* and *CIN3* homologs (Figs S2, S3). Also, the *miR319* binding site exclusive for *CIN1* and *CIN3* proteins is recovered as part of motif 5 in the former and motif 11 in the latter (Figs S2, S3).

Expression of class II TCP genes by RT-PCR

Class II TCP gene expression was first evaluated in flowering apices including floral stages S0–S5 and floral buds between S6 and S8 that range in length between 1–2 cm and are relatively easy to dissect into dorsal and ventral perianth portions (Fig. S4). All class II TCP genes were amplified at 30 cycles with the exception of *AfimCIN2*, which was amplified and detected only after 35 cycles. From all genes tested, only *AfimCIN2* lacks expression in flowering shoots having the early flower developmental stages (S0–S5). In older flowers, *AfimCYC* and *AfimCIN2* were similarly expressed in the dorsal and ventral portions of the perianth.

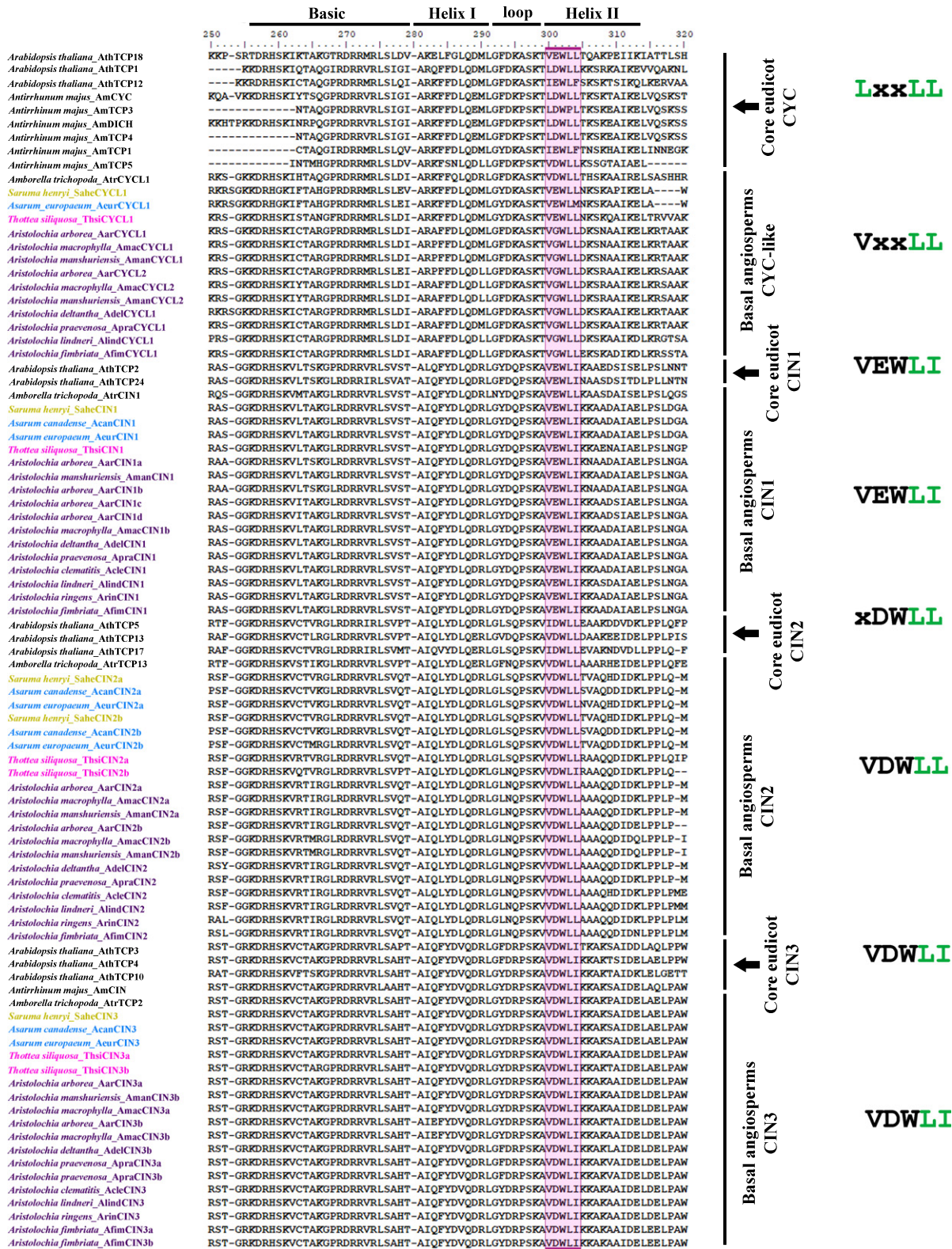


Fig. 4 TCP protein domain alignment for selected sequences included in the phylogenetic analysis presented in Fig. 2. The pink box corresponds to the first five amino acids of the second helix of the TCP domain, putatively in charge of protein interactions. Sequences and their variable sites (marked with 'x') are shown to the right for each group of class II TCP clades. *CYC*, *CYCLOIDEA* genes; *CYC-like*, *CYCLOIDEA-LIKE* genes; *CIN1*, *CIN2*, *CIN3*, *CINCINNATA* 1, 2 and 3.

On the other hand, *AfimCIN1*, *AfimCIN3a* and *AfimCIN3b* were differentially expressed between the ventral and the dorsal portions of the perianth (Fig. S4). We decided to proceed with detailed *in situ* hybridization studies of the sole *CYC* representative, *AfimCYC*, and the differentially expressed *CIN* representatives, *AfimCIN1*, *AfimCIN3a* and *AfimCIN3b*.

Expression of *AfimCYC*

AfimCYC, the only *CYC* homolog found in the *A. fimbriata* transcriptome, is expressed in the shoot apical meristem (SAM), in the intervacular areas of the leaves (Fig. 5a,b), and throughout the perianth in the early floral buds when sepals are starting to develop at S1 (Fig. 5a) as well as during the elongation of the medial sepal at S2 (Fig. 5a,c). Expression of *AfimCYC* is also evident in the stamens and the ovary during their initiation at S3 (Fig. 5d,e). At S4, *AfimCYC* remains homogeneously expressed in the perianth, showing the same expression in the ventral and the dorsal portions of the limb (Fig. 5f,g), the tube (Fig. 5h), and the utricle (Fig. 5i) as well as in the ovary (Fig. 5j). At S5, when stigmas have already elongated in the gynostemium, *AfimCYC* is expressed strongly in the stamens, the stigmatic tips, the ovary and the perianth, especially in the growing tips of the limb and in the expanding utricle (Fig. 5k). A similar expression can be detected in the dorsal and ventral sectors of the flower (Fig. 5k). At S6, *AfimCYC* expression in the gynostemium becomes restricted to the stamens and the boundary between stamens and stigmas (Fig. 5l,m). At this same stage, *AfimCYC* continues to be expressed in the ovary and the growing perianth with a slightly higher signal detected in the ventral portion of the perianth, especially in the limb and the tube (Fig. 5m). During ovary maturation, *AfimCYC* is expressed in the closing carpel margins, around the vascular traces of the carpels, and the ovules, specifically in the integuments (Fig. 5n). Finally, *AfimCYC* is also detected in the accessory buds, occasionally forming next to the axillary floral buds (Fig. S5). These buds are frequently suppressed in development and rarely enter organogenesis.

Expression of *AfimCIN1*

AfimCIN1 is expressed in the SAM and the leaves, especially in their growing tips, as well as the perianth in the early floral buds when sepals are starting to develop at S1 (Fig. 6a) and during the elongation of the medial sepal at S2 (Fig. 6a,b); its expression in the leaf intervacular areas is reduced (Fig. 6a). Expression of *AfimCIN1* appears strongest in the stamens and the ventral sector of the flower at S3 and S4 (Fig. 6c,d). At S5 *AfimCIN1* is localized at the tip of the flower (i.e. the limb), the ventral portion of the perianth, the stamens, the transmitting tract tissue, and the abaxial portions of the stigmatic tips (Fig. 6e,f). Similar expression patterns are maintained for *AfimCIN1* at S6 with increased expression in the developing placenta (Fig. 6g–i) and the developing ovules (Fig. 6j). *AfimCIN1* expression is maintained in fully developed ovules, particularly in the funiculus, the growing margins of the integuments and the nucellus (Fig. 5k).

Expression of *AfimCIN3a* and *AfimCIN3b*

AfimCIN3a is expressed in the SAM, in the leaves, especially in the tips and the adaxial surface, with reduced expression in the intervacular areas (Fig. 7a–c). *AfimCIN3a* is expressed homogeneously in the youngest floral buds at S1 and S2 (Fig. 7a,b). Between S3 and S4 a higher expression of *AfimCIN3a* can be seen in the ventral portion of the limb (Fig. 7d,e) and the tube (Fig. 7d,f) while it is continuously expressed homogeneously in stamens and ovary (Fig. 7d). The same pattern continues to be found in S5 and S6, with *AfimCIN3a* present in the stamens and the ovary, and a marked expression in the ventral portion of the limb (Fig. 7g). This is more obvious in S7 where expression is restricted to the ventral portion of the limb and is completely absent from the dorsal part (Fig. 7h). At this stage *AfimCIN3a* is expressed in the stamens, the abaxial portions of the stigmas, the ovary, the placenta and the young ovules (Fig. 7i,j), while expression continues in mature ovules, in both integuments, the nucellus, as well as in the abaxial portion of the carpel margins (Fig. 7k). Finally, *AfimCIN3a* is also present in the accessory dormant buds (Fig. 7l).

By comparison, *AfimCIN3b* has lower expression levels than *AfimCIN3a*. *AfimCIN3b* is active in the SAM, the tips of the leaves and the young floral buds during sepal initiation at S1 and during the elongation of the medial sepal at S2 (Fig. 8a). At S3 and S4 *AfimCIN3b* appears to be preferentially expressed in the ventral portion of the limb, and also in the stamens and the ovary (Fig. 8b–d). Expression of *AfimCIN3b* in the perianth is seen only in the ventral part of the flower continuing until S5 and S6 (Fig. 8e,f), as well as in the ovary, especially in the outer epidermis and in the ovules, including the integuments and the nucellus (Fig. 8g).

Expression of *AfimHIS4*

In order to investigate whether the expression of *AfimCIN1*, *AfimCIN3a* and *AfimCIN3b* is correlated with the promotion or reduction of cell division, we tested the expression of *HISTONE4* during floral development in *A. fimbriata*. As a cell division marker, *HIS4* is expressed during active cell division. *AfimHIS4* is expressed in the surrounding areas of the SAM, the tips and the adaxial surfaces of the young leaves, as well as the floral buds at S1 (Fig. 9a–c). *AfimHIS4* remains active in the intervacular areas of the expanding leaves (Fig. 9b). From S1 to S4, *AfimHIS4* can be detected in the elongating dorsal sepal and more strongly in the ventral sepals, as well as in stamens and in the ovary (Fig. 9a–e). However, from S5 onwards, *AfimHIS4* is preferentially located in the ventral portion of the perianth, particularly at the level of the limb (Fig. 9f–i). Finally, *AfimHIS4* is also expressed in the stamens and the young ovules (Fig. 9j; data not shown).

Discussion

TCP plant transcription factors are characterized by a noncanonical bHLH DNA-binding domain and have been linked with a

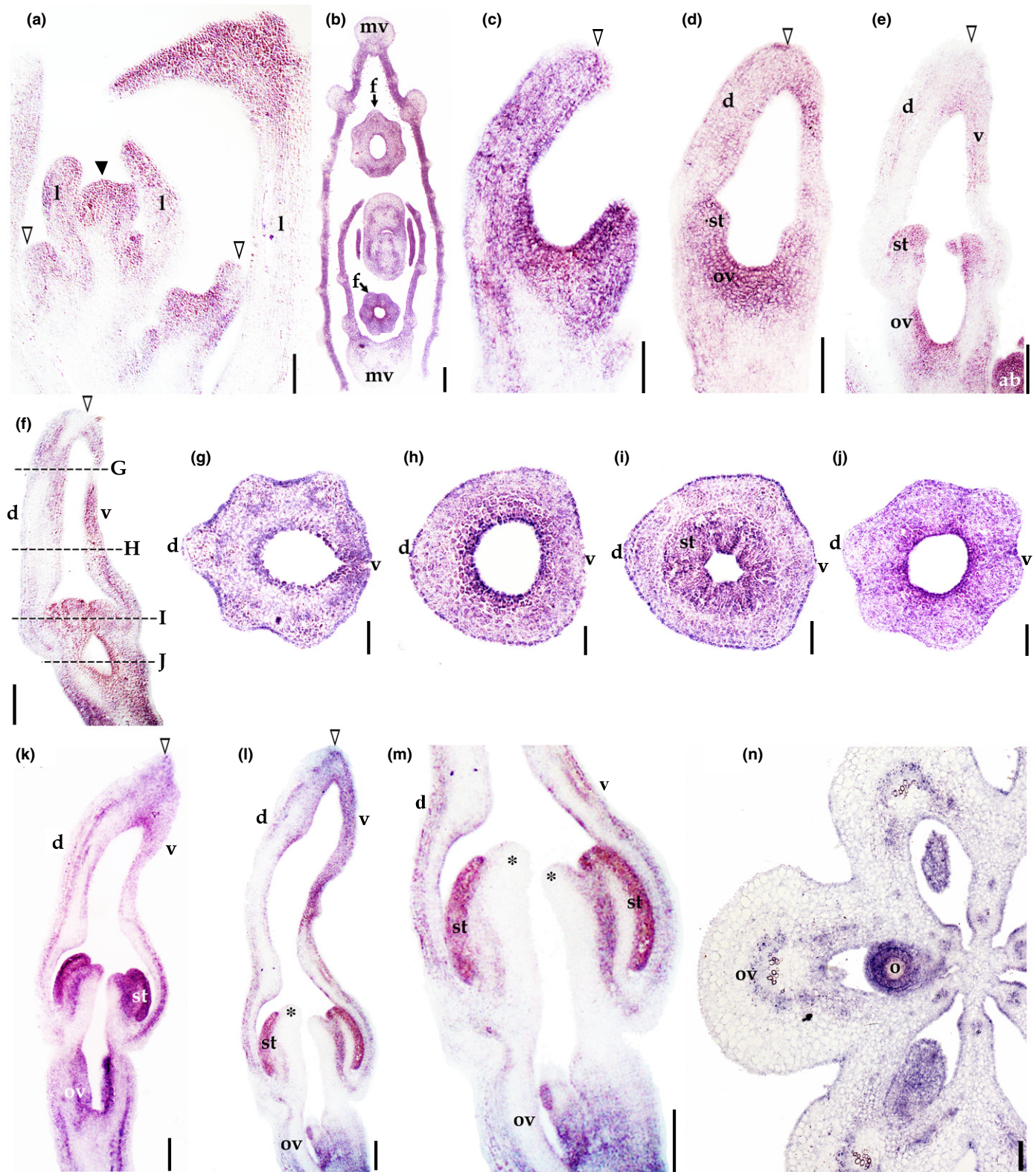


Fig. 5 *In situ* hybridization expression of *AfimCYC*. (a) Longitudinal section of the flowering shoot apex. (b) Transverse section of the flowering shoot apex showing two axillary flowers (f) and their subtending leaves. (c–e) Longitudinal sections of one S2 (c) and two S3 flower primordia (d, e). (f) Longitudinal section of one S4 flower. (g–j) Transverse sections at the level of the limb (g), tube (h), utricle (i) and ovary (j). (k) longitudinal section of one S5 flower. (l, m) Longitudinal section of one S6 flower (l) and details of the gynostemium and the ovary (m). (n) Transverse section of the ovary with ovules during integument differentiation at S9: d, dorsal portion of the flower; f, flower or floral bud; l, leaf; mv, midvein of the leaf; o, ovule; ov, ovary; st, stamens or stamen primordia; v, ventral portion of the flower. Black arrowhead points to the shoot apical meristem; white arrowheads point to the medial sepal tip; asterisks (*) point to stigmatic lobes. Bars: 100 μ m (a, b, e–n); 50 μ m (c, d).

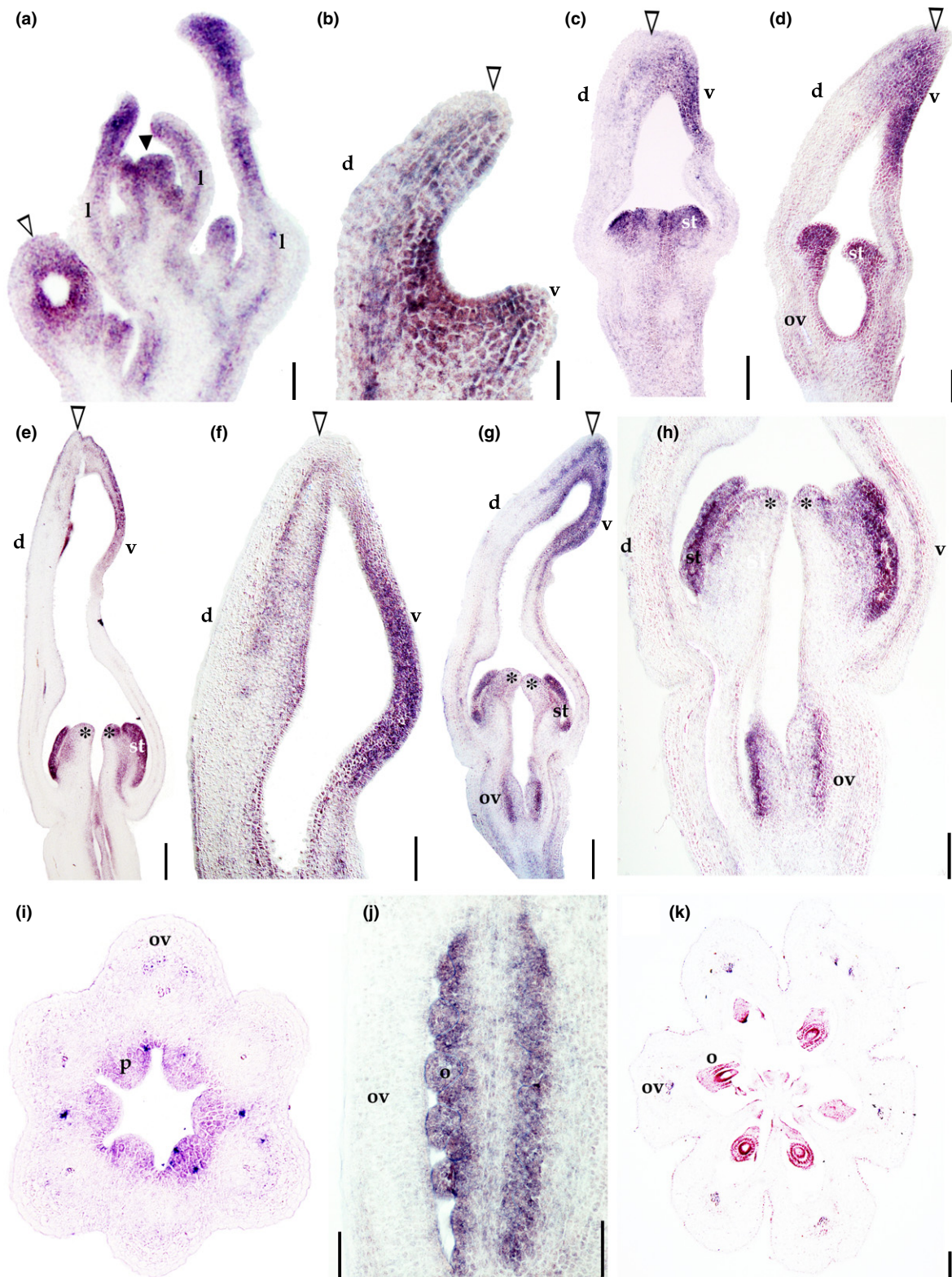


Fig. 6 *In situ* hybridization expression of *AfimCIN1*. (a) Longitudinal section of the flowering shoot apex with floral bud at stages S0, S1 and S2. (b–e) Longitudinal sections of floral buds at stages S2 (b), S3 (c), S4 (d) and S5 (e). (f) Detail of limb at stage S5. (g, h) Longitudinal section of the floral bud at stage S6 (g) and detail of ovary and gynostemium (h). (i) Transverse section of the ovary with the placenta at stage S5. (j) Longitudinal section of the ovary at stage S6 with the placenta and ovule primordia. (k) Transverse section of the ovary with ovules during integument differentiation at stage S9: d, dorsal portion of the flower; l, leaf; o, ovule; ov, ovary; p, placenta; st, stamens or stamen primordia; v, ventral portion of the flower. Black arrowhead points to the shoot apical meristem; white arrowheads point to the medial sepal tip; asterisks (*) point to stigmatic lobes. Bars: 100 μm (a, c, d, f, h, i, l); 200 μm (e, g); 50 μm (b, j).

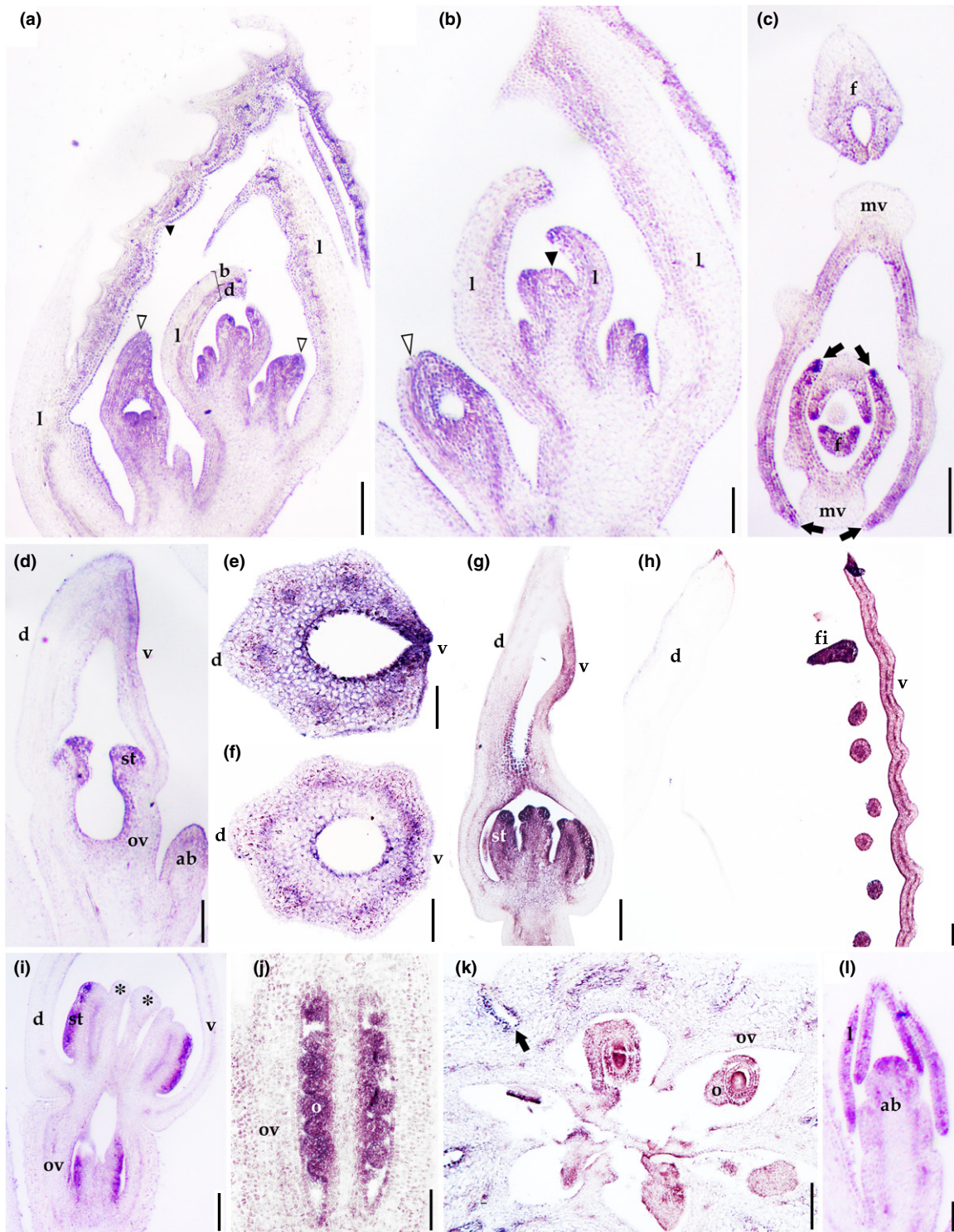


Fig. 7 *In situ* hybridization expression of *AfimCIN3a*. (a) Longitudinal section of the flowering shoot apex with a fully formed leaf (a), b indicates the abaxial leaf flank, d, indicates the adaxial leaf flank. (b) Detail of a shoot apex with floral buds at stages S0, S1 and S2. (c) Transverse section of a flowering shoot apex with three young leaves and their respective axillary floral buds; arrows point to leaf margins. (d) Longitudinal section of the floral bud at stage S4. (e, f) Transverse sections at the level of the limb (e) and the tube (f) at stage S4. (g) Longitudinal section of a S5 flower. (h–j) Longitudinal sections of the limb (h), utricle and gynostemium (i) and ovary (j) at stage S7. (k) Transverse section of the ovary with ovules during integument differentiation at stage S9; arrow points to intercarpellary furrow. (l) Longitudinal section of the accessory dormant buds: ab, accessory bud; d, dorsal portion of the flower; f, flower or floral bud; fi, fimbriae; l, leaf; o, ovule; ov, ovary; st, stamens or stamen primordia; v, ventral portion of the flower. Black arrowhead points to the shoot apical meristem; white arrowheads point to the medial sepal tip; asterisks (*) point to stigmatic lobes. Bars: 250 μm (a, i); 50 μm (e, f); 100 μm (b–d, g, h, j, k, l).

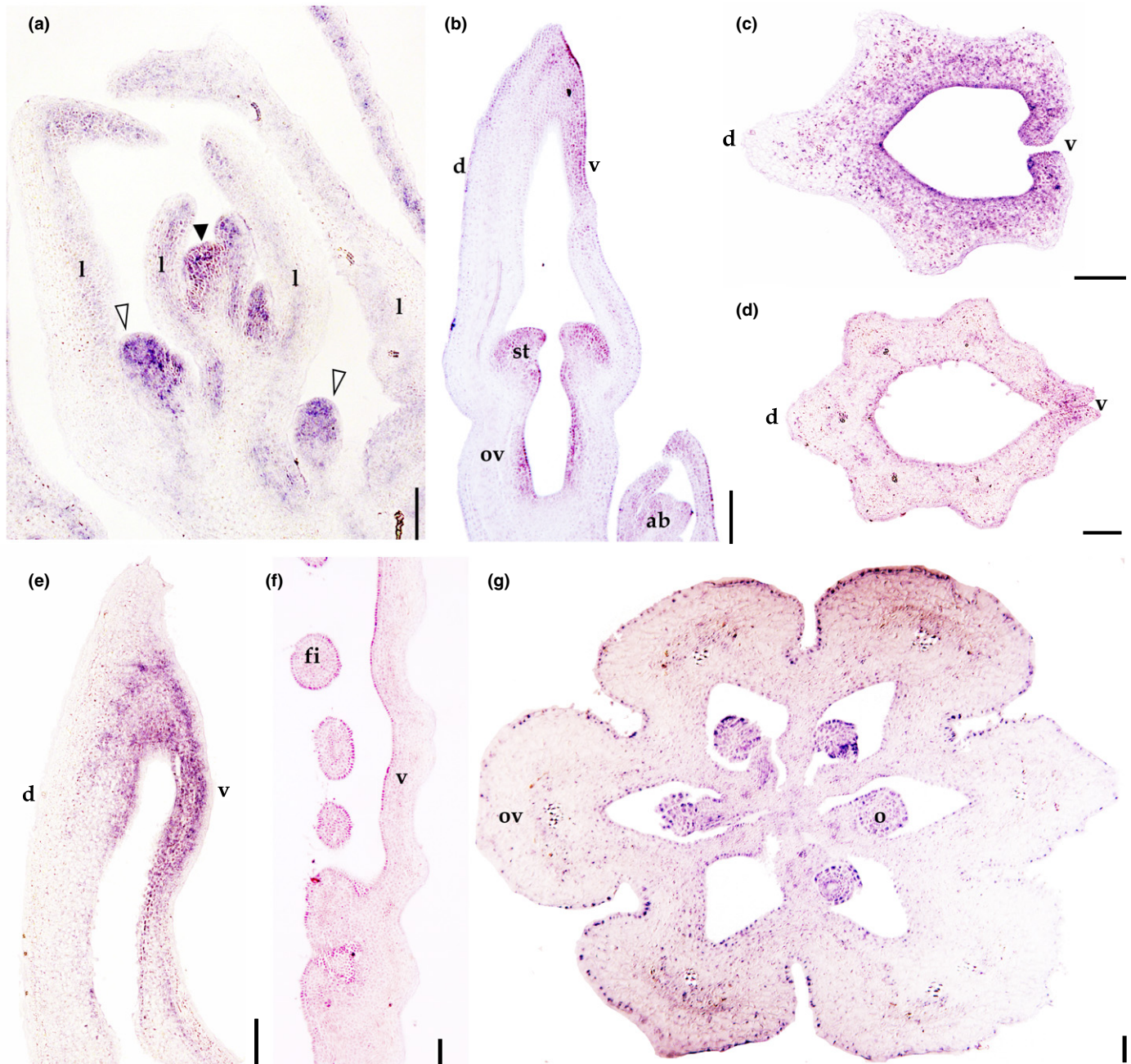


Fig. 8 *In situ* hybridization expression of *AfimCIN3b*. (a) Longitudinal section of a shoot apex with floral primordia at stages S0, S1 and S2. (b–d) Longitudinal (b) and transverse sections at the level of the distal (c) and proximal (d) portions of the limb in a S3 flower. (e) Detail of the limb at stage S5. (f) Detail of the dorsal portion of the flower at stage S7. (g) Transverse section of the ovary with ovules during integument differentiation at stage S9: ab, accessory bud; d, dorsal region of the flower; f, flower; l, leaf; o, ovule; ov, ovary; st, stamen primordia; v, ventral region of the flower. Black arrowhead points to the shoot apical meristem; white arrowheads point to the medial sepal tip. Bars, 50 μm (a–g).

plethora of developmental roles. Based on phylogenetic analyses as well as detailed sequence analyses and three-dimensional predictions for protein assembly, class I (or TCP-P) and class II (or TCP-C) TCP genes have been identified (Cubas *et al.*, 1999; Cubas, 2002). Class II TCP genes have been further categorized into *CIN* genes present across land plants and *CYCLOIDEA (CYC)/TEOSINTE BRANCHED1 (TBI)* genes specific to angiosperms (Navaud *et al.*, 2007). The functional characterization of *CYC/TBI* lineage members has shown a close

relationship with the control of cell proliferation in different plant organs in several species. For instance, the *Arabidopsis AthTCP18* and *AthTCP12* (also named *BRC1* and *BRC2* respectively) control shoot branching (Aguilar-Martínez *et al.*, 2007). Similarly, *TBI* is expressed in axillary meristems and is responsible for suppressing branch growth in maize (Doebley *et al.*, 1995, 1997; Doebley, 2004). The *Oryza sativa* *CYC* homolog *REP1* contributes to asymmetric growth of the flower-promoting cell division in the palea (Yuan *et al.*, 2009). Finally, *CYC* and its

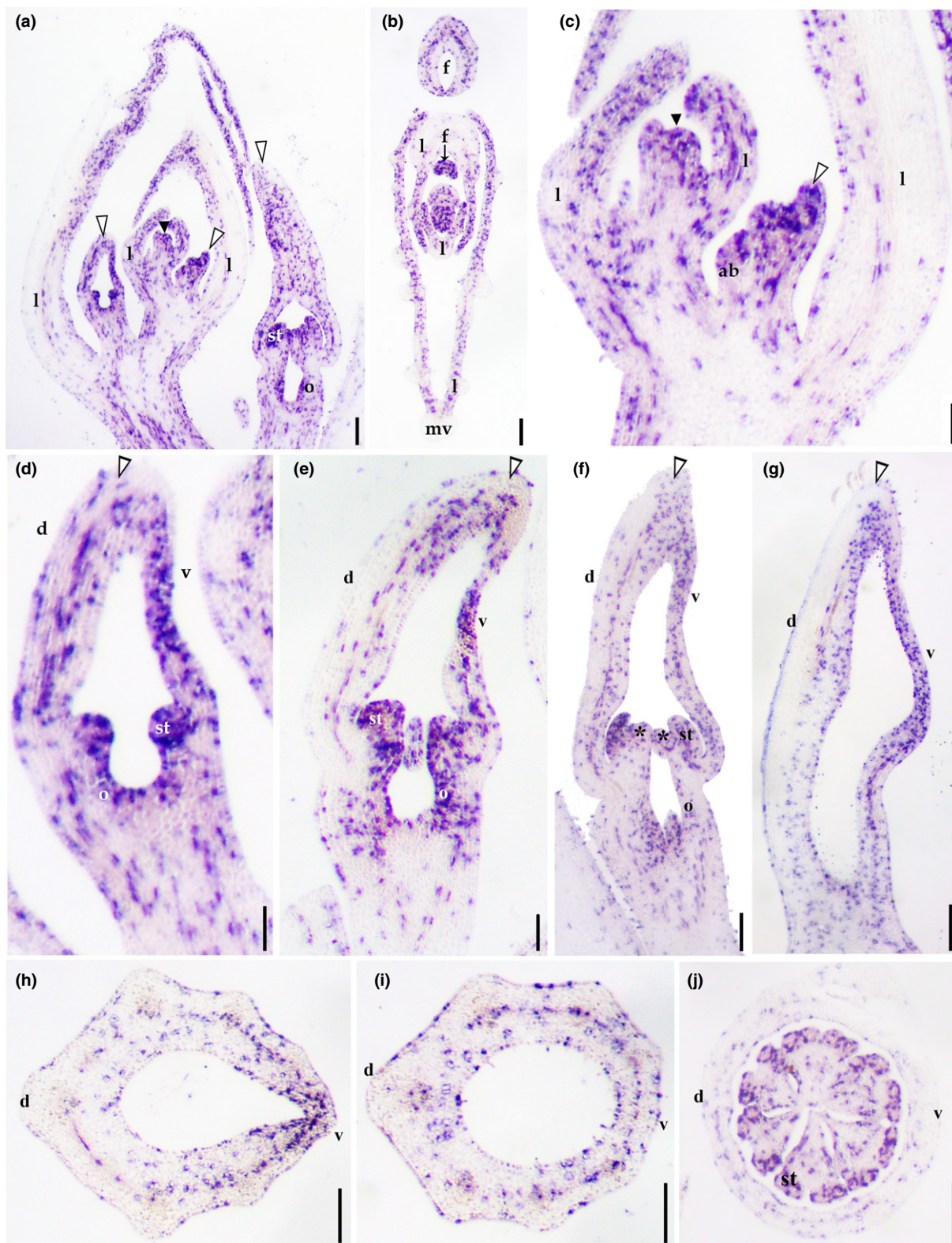


Fig. 9 *In situ* hybridization expression of *AfimHIS4*. (a) Longitudinal section of the flowering shoot apex with S0–S5 floral bud stages as well as leaf primordia and fully formed leaves. (b) Transverse section of the flowering shoot apex with focus on the expanding margins of the leaves and the axillary flowers. (c) Detail of the shoot apical meristem (SAM) and the floral buds at S1 and S2 during perianth initiation and elongation. (d–g) Longitudinal sections of floral buds at S2 (d), S3 (e), S4 (f) and S5 (g). (h–j) Transverse section of the limb (h), tube (i) and utricle (j) at stage S5. ab, accessory bud; d, dorsal portion of the flower; f, flower; l, leaf; o, ovule; ov, ovary; st, stamens or stamen primordia; v, ventral portion of the flower. Black arrowhead points to the shoot apical meristem; white arrowheads point to the medial sepal tip; asterisks (*) point to stigmatic lobes. Bars, 150 μ m (a–c); 100 μ m (d–j).

paralog *DICH* are expressed in the so-called dorsal portion of the *A. majus* flower where it controls cell proliferation, resulting in differential dorsiventral growth and the formation of bilateral flowers (Luo *et al.*, 1996, 1999).

CINCINNATA genes have been only functionally studied in *A. majus* and *A. thaliana*. *CIN* genes are distinguished based on their regulation by *miR319*, as follows: *CIN1* (with the *Arabidopsis* *TCP2* and *TCP24*) and *CIN3* (including the canonical *CIN*, and the *Arabidopsis* *TCP3*, *TCP4* and *TCP10*) are regulated by *miR319* (also known as *miRJA*W), whereas members of the *CIN2* clade (including the *Arabidopsis* *TCP5*, *TCP13* and *TCP17*) are *miR319* resistant (Li, 2015). Most of the *CIN* genes characterized so far play roles in the control of cell division during leaf development; thus, downregulation in *Arabidopsis* causes larger, crinkled, over-proliferating leaves (Palatnik *et al.*, 2003; Efroni *et al.*, 2008). The canonical *CIN* in *A. majus* is differentially expressed in both leaves and flowers. In leaves, it is specifically activated in the adaxial side, more strongly in margins than in the mesophyll, and it is lacking in the vascular tissue (Nath *et al.*, 2003). Because *cin* mutants in snapdragon are no longer flat and have excess growth in the lamina margins, *CIN* is thought to negatively control cell proliferation by promoting the transition from cell division to cell growth (Nath *et al.*, 2003). Conversely, the *cin* mutant flowers have green, shorter petals with epidermal flat cells, which indicates that *CIN* promotes cell division and conical cell differentiation in distal portions of the petals (Crawford *et al.*, 2004).

The exact mechanisms by which *TCP* genes promote or repress cell proliferation in different organs are not fully understood. Several studies have pointed out that changes in function rely on specific protein interactions established by short regions inside the bHLH domain, as well as unique acidic motifs downstream (Kosugi & Ohashi, 2002; Li *et al.*, 2005, 2011; Viola *et al.*, 2011; Danisman *et al.*, 2012). For instance, the LxxLL motif in the second helix within the bHLH domain has proven to be key for the interactions between transcription factors and co-activators in both plants and animals (Heery *et al.*, 1997). An intact LxxLL motif is found only in some core eudicot CYC2 proteins, including the canonical CYC, and it has been identified as critical for the role of *CYC2* homologs to establish early bilateral floral symmetry (Horn *et al.*, 2015). However, other core eudicot CYC and the non-core eudicot CYC-like proteins, including the *Aristolochiaceae* homologs, have a VxxLL motif (Fig. 4; Horn *et al.*, 2015). It is unclear whether this shift in sequence has a functional effect, as neither the original VxxLL AarCYC-like proteins nor the LxxLL modified version of this protein results in obvious changes in cell division in the petals (i.e. smaller petals) in *Arabidopsis* after heterologous overexpression (Horn *et al.*, 2015). The homogeneous and low expression of *CYC-like* homologs in *A. arborea* further suggest that *CYC* homologs are not involved in the differential cell division and expansion of the *Aristolochia* bilateral perianth (Horn *et al.*, 2015). Our data in *A. fimbriata* show a higher expression of the only *CYC-like* gene compared with the two copies *AarCYCL1* and *AarCYCL2* in *A. arborea*. However, although expression is higher, *AfimCYC* expression is uniform between the dorsal and the ventral portions of the floral

primordia and during early sepal initiation and elongation, like in *A. arborea* (Fig. 5; Horn *et al.*, 2015). These data indicate that *AfimCYC* contributes neither to differential sepal elongation nor to the acquisition of early bilateral symmetry in the floral bud. Interestingly, expression of *AfimCYC* increases towards the ventral portion of the flower after S5, both in the utricle and in the limb, and coincides with augmented *AfimHIS4* accumulation. This suggests that *AfimCYC* could contribute to the increased rates of cell division in the ventral portion of the flower in preanthesis as well as the curvature of the perianth to some extent in the later stages of flower development (Fig. 5k,l). Differences observed between *A. fimbriata* and *A. arborea* can be a result of changes in copy number of *CYC* genes between subgenus *Aristolochia* (single copy) and subgenus *Siphisia* (with two paralogs).

As for the *CIN* homologs, our data confirm two consecutive duplication events resulting in three clades with representative genes from all angiosperms, instead of the single duplication previously reported (Madrigrál *et al.*, 2017; Suárez-Baron *et al.*, 2019). Only a few *CIN* genes have been functionally characterized, even though they are at the core of cell division processes. From our phylogenetic analyses we can conclude that *miR319a* regulation is ancestral in *CIN* genes and it was lost in the *CIN2* clade. A comparison between the *CIN* proteins shows a VxWLIx motif at the beginning of the second helix. Interestingly, the VEWLI motif present in *CIN1* proteins as well as the VDWLI from *CIN3* proteins (Fig. 3) match 100% with plant Cyclin proteins (Figs S1, S2, S6). Because these motifs have been shown to drive heterodimerization such sequence similarity opens the possibility that *Cyclin* genes can interact with *TCP* proteins given that they share identical motifs (Danisman *et al.*, 2013). Previously only *CYC* genes had been shown to directly or indirectly suppress *cyclinD3b* in staminodes of *Antirrhinum* (Gaudin *et al.*, 2000). However, it is clear that developmental regulators are intertwined with the control of cell proliferation and such sequence similarities will need to be further addressed to test their contribution to protein interactions.

Our expression data for *AfimCIN1*, *AfimCIN3a* and *AfimCIN3b* show homogeneous expression in the floral bud at early developmental stages followed by a differential dorsiventral expression during perianth development and growth until preanthesis. More specifically, *CIN* transcripts become restricted to the ventral portion of the perianth and more strongly in the limb compared with the tube or the utricle (Figs 6–8). The limb is the most actively growing portion of the perianth in a number of species of *Aristolochia* subgenus *Aristolochia* (González & Stevenson, 2000). Specifically, the ventral portion of the perianth probably corresponds to the free marginal meristems of the lateral sepals where most of the active cell division occurs, as shown by the accumulation of *AfimHIS4* (Figs 6–9). This coincides with the observation by Suárez-Baron *et al.* (2019) that *CIN* genes are more highly expressed in the limb of *A. ringens* when compared with the tube or the utricle. *CIN1* and *CIN3* genes have putative *miR319*-binding sites in their transcripts and their expression is in fact mutually exclusive with *miR319*, which has been reported with higher expression in the utricle (Suárez-Baron *et al.*, 2019).

Altogether, the data suggest that *CIN* genes, and more strongly *AfimCIN1* and *AfimCIN3a*, are probably promoting the differential rates of cell division in the ventral portion of the limb contributing to the perianth differential growth and its bilateral symmetry starting in stage S3 until preanthesis (Figs 6, 7).

TCP genes can activate *NGATHA* genes during gynoecium development (Ballester *et al.*, 2015) and play key roles in ovule cell division in orchids (Lin *et al.*, 2016), fruit patterning in *Arabidopsis* and fruit ripening in tomato (Parapunova *et al.*, 2014). Because *AfimCYC* and *AfimCIN* overlap with *AfimHIS4* expression in floral meristems, stamens and their boundary with the stigmatic tips, as well as growing ovules, it is likely that both class II *TCP* homologs in *Aristolochia* play roles in promoting and maintaining cell division in these organs.

The expression recorded for class II *TCP* genes in the SAM and the adaxial side and the intervascular leaf tissue is very similar to those reported in other *TCP* genes, including *CIN* in *A. majus*. The active expression of *TCP* genes in the elongating vegetative and floral meristems and leaves suggests that class II *TCP* genes in *Aristolochia* act in the control of proper shoot morphogenesis. *TCP* control of SAM morphogenesis occurs in *Arabidopsis* by negatively regulating boundary-specific genes, such as the *CUP SHAPED COTYLEDON (CUC)* genes (Koyama *et al.*, 2007); however, no studies of *CUC* expression have been done in *A. fimbriata*. On the other hand, the expression in leaves must be interpreted with caution. Although expression of class II *TCP* genes in *A. fimbriata* leaves overlaps with *AfimHIS4*, which suggests a role in promoting cell division, it is likely that, as it occurs in *A. majus*, the *TCP* genes are fine tuning the cell division rates and the transition from cell division to cell growth (Nath *et al.*, 2003; Crawford *et al.*, 2004). Nevertheless, functional analyses will have to confirm how these putative roles occur in vegetative and floral organs, as *CIN* genes overlap in expression with *HIS4* and *Cyclin* genes in leaves and petals yet exhibit opposite roles in promoting or repressing cell division in the two.

In conclusion, the constitutive expression patterns of class II *TCP* genes during early flower development in *Aristolochia* suggest that either they do not control the establishment of the bilateral symmetry caused by differential sepal growth or they need overlapping partners that provide spatial growth differences early in flower development. It is possible that other unidentified genetic mechanisms control the early establishment of bilateral perianth symmetry in *Aristolochia*, the only lineage outside the monocots and eudicots exhibiting such a feature. Nonetheless, class II *TCP* factors are probably key to promoting and maintaining differential mid- and late perianth growth by positively regulating cell division in the ventral portion of the limb. The latter role could be achieved by promoting downstream cell division genes through the direct action of the *miR319*-targeted *CIN1* and *CIN3* genes. *CYC* and *CIN* expression in *A. fimbriata* also suggests that they can play key roles in controlling cell division patterns in leaves, gynoecium and ovules. However, whether these promote or repress proliferation will have to wait for functional analyses to be optimized in the emerging plant model *A. fimbriata*.








Acknowledgements

We thank Anny Garcés Palacio, Sarita Muñoz, Pablo Pérez-Mesa (Universidad de Antioquia, Colombia), Cecilia Zumajo-Cardona (The New York Botanical Garden), Ana Berbel and Clara Inés Ortiz-Ramírez (Instituto de Biología Molecular y Celular de Plantas, CSIC-UVP, Valencia, Spain) for photographs and assistance during laboratory work. We also thank Sebastián González (Massachusetts College of Art and Design) for taking some of the photographs in Figs 1 and 2. Thanks are also due to the Dresden Junior Fellowship for allowing the visiting professor fellowship of NPM to the Technische Universität Dresden during 2019. This research was funded by Estrategia de Sostenibilidad 2018–2019 the Convocatoria Programáticas 2017–2018 (code 2017-16302), and the 2018–2019 Fondo de Internacionalización (code 2019-26230) from the Universidad de Antioquia, the iCOOP + 2016 grant COOPB20250 from Centro Superior de Investigación Científica, CSIC and the ExpoSEED (H2020.MSCA-RISE-2015-691109) EU grant. Open access funding enabled and organized by Projekt DEAL.

Author contributions

NP-M and FG planned and designed the research and wrote the manuscript. NP-M, YM and JFA performed experiments in the laboratories of BAA, SW, CN and CF. All authors analyzed data and revised and approved the manuscript.

ORCID

Juan F. Alzate  <https://orcid.org/0000-0003-2578-4609>
 Barbara A. Ambrose  <https://orcid.org/0000-0002-9617-0148>
 Cristina Ferrándiz  <https://orcid.org/0000-0002-2460-1068>
 Favio González  <https://orcid.org/0000-0001-5716-9278>
 Yesenia Madrigal  <https://orcid.org/0000-0001-6992-3645>
 Christoph Neinhuis  <https://orcid.org/0000-0001-9965-4394>
 Natalia Pabón-Mora  <https://orcid.org/0000-0003-3528-8078>

References

- Aguilar-Martínez JA, Poza-Carrión C, Cubas P. 2007. *Arabidopsis* BRANCHED1 acts as an integrator of branching signals within axillary buds. *Plant Cell* 19: 458–472.
- Almeida J, Rocheta M, Galego L. 1997. Genetic control of flower shape in *Antirrhinum majus*. *Development* 124: 1387–1392.
- Altschul SF, Gish W, Miller W, Myers EW, Lipman DJ. 1990. Basic local alignment search tool. *Journal of Molecular Biology* 215: 403–410.
- Ambrose BA, Lerner DR, Ciceri P, Padilla CM, Yanofsky MF, Schmidt RJ. 2000. Molecular and genetic analyses of the *Silky1* gene reveal conservation in floral organ specification between eudicots and monocots. *Molecular Cell* 5: 569–579.
- Ballester P, Navarrete-Gómez M, Carbonero P, Oñate-Sánchez L, Ferrándiz C. 2015. Leaf expansion in *Arabidopsis* is controlled by a TCP-NGA regulatory module likely conserved in distantly related species. *Physiologia Plantarum* 155: 21–32.
- Bartlett ME, Specht CD. 2011. Changes in expression pattern of the *TEOSINTE BRANCHED1*-like genes in the Zingiberales provide a mechanism for

- evolutionary shifts in symmetry across the order. *American Journal of Botany* 98: 227–243.
- Bliss BJ, Wanke S, Bakarar A, Ayyampalayam S, Wickett N, Wall PK *et al.* 2013. Characterization of the basal angiosperm *Aristolochia fimbriata*: a potential experimental system for genetic studies. *BMC Plant Biology* 13: 13.
- Busch A, Zachgo S. 2007. Control of corolla monosymmetry in the Brassicaceae *Iberis amara*. *Proceedings of the National Academy of Sciences, USA* 104: 16714–16719.
- Citerne H, Jabbour F, Nadot S, Damerval C. 2010. The evolution of floral symmetry. In: Kader JC, Delseny M, eds. *Advances in botanical research*. London UK: Academic Press, 85–137.
- Citerne H, Reyes E, LeGuilloux M, Delannoy E, Simonnet F, Sauquet H, Weston PH, Nadot S, Damerval C. 2016. Characterization of CYCLOIDEA-like genes in Proteaceae, a basal eudicot family with multiple shifts in floral symmetry. *Annals of Botany* 119: 367–378.
- Corley SB, Carpenter R, Copey L, Coen E. 2005. Floral asymmetry involves an interplay between TCP and MYB transcription factors in *Antirrhinum*. *Proceedings of the National Academy of Sciences, USA* 102: 5068–5073.
- Crawford BCW, Nath U, Carpenter R, Coen ES. 2004. *CINCINNATA* controls both cell differentiation and growth in petal lobes and leaves of *Antirrhinum*. *Plant Physiology* 135: 244–253.
- Cubas P. 2002. Role of TCP genes in the evolution of morphological characters in angiosperms. In: Cronk QCB, Bateman RM, Hawkins JA, eds. *Developmental genetics and plant evolution 65*. London, UK: The Systematics Association, 247–266.
- Cubas P, Lauter N, Doebley J, Coen E. 1999. The TCP domain: a motif found in proteins regulating plant growth and development. *The Plant Journal* 18: 215–222.
- Damerval C, Citerne H, Conde e Silva N, Deveaux Y, Delannoy E, Joets J, Simonnet F, Staedler Y, Schöenberger J, Yansouni J *et al.* 2019. Unraveling the developmental and genetic mechanisms underpinning floral architecture in Proteaceae. *Frontiers in Plant Science* 10: <https://doi.org/10.3389/fpls.2019.00018>
- Damerval C, Citerne H, Le Guilloux M, Domenichini S, Duthel J, de Craene LR, Nadot S. 2017. Asymmetric morphogenetic cues along the transverse plane: shift from dissymmetry to zygomorphy in the flower of Fumarioideae. *Annals of Botany* 100: 391–402.
- Damerval C, LeGuilloux M, Jager M, Charon C. 2007. Diversity and evolution of *CYCLOIDEA*-like TCP genes in relation to flower development in Papaveraceae. *Plant Physiology* 143: 759–772.
- Danisman S, Van Der Wal F, Dhondt S, Waites R, de Folter S, Bimbo A, van Dijk AD, Muino JM, Cutri L, Dornelas MC *et al.* 2012. Arabidopsis class I and class II TCP transcription factors regulate jasmonic acid metabolism and leaf development antagonistically. *Plant Physiology* 159: 1511–1523.
- Danisman S, van Dijk ADJ, Bimbo A, van der Wal F, Hennig L, de Folter S, Angenent GC, Immink RGH. 2013. Analysis of functional redundancies within the Arabidopsis TCP transcription factor family. *Journal of Experimental Botany* 64: 5673–5685.
- Doebley J. 2004. The genetics of maize evolution. *Annual Reviews in Genetics* 38: 37–59.
- Doebley J, Stec A, Gustus C. 1995. *TEOSINTE BRANCHED1* and the origin of maize: evidence for epistasis and the evolution of dominance. *Genetics* 141: 333–346.
- Doebley J, Stec A, Hubbard L. 1997. The evolution of apical dominance in maize. *Nature* 86: 485–488.
- Efroni I, Blum E, Goldshmidt A, Eshed Y. 2008. A protracted and dynamic maturation schedule underlies *Arabidopsis* leaf development. *Plant Cell* 20: 2293–2306.
- Elomaa A, Zhao Y, Zhang T. 2018. Flower heads in Asteraceae – recruitment of conserved developmental regulators to control the flower-like inflorescence architecture. *Horticulture Research* 5: 36.
- Endress PK. 2012. The immense diversity of floral monosymmetry and asymmetry across angiosperms. *Botanical Review* 78: 345–397.
- Ferrández C, Liljegren SJ, Yanofsky MF. 2000. Negative regulation of the *SHATTERPROOF* genes by *FRUITFULL* during *Arabidopsis* fruit development. *Science* 289: 436–438.
- Galego L, Almeida J. 2002. Role of *DIVARICATA* in the control of dorsoventral asymmetry in *Antirrhinum* flowers. *Genes and Development* 16: 880–891.
- Gaudin V, Lunness PA, Robert PR, Towers M, Riou-Khamlichi C, Murray JAH *et al.* 2000. The expression of *D-Cyclin* genes defines distinct developmental zones in snapdragon apical meristems and is locally regulated by the *Cycloidea* gene. *Plant Physiology* 122: 1137–1148.
- González F, Pabón-Mora N. 2015. Trickery flowers: the extraordinary chemical mimicry of *Aristolochia* to accomplish deception to its pollinators. *New Phytologist* 206: 10–13.
- González F, Stevenson DW. 2000. Perianth development and systematics of *Aristolochia*. *Flora* 195: 370–391.
- Heery DM, Kalkhoven E, Hoare S, Parker MG. 1997. A signature motif in transcriptional co-activators mediates binding to nuclear receptors. *Nature* 387: 733–736.
- Hileman LC. 2014. Trends in flower symmetry evolution revealed through phylogenetic and developmental genetic advances. *Philosophical Transactions of the Royal Society B: Biological Sciences* 369: 1–10.
- Hoang DT, Chernomor O, Von Haeseler A, Minh BQ, Vinh LS. 2018. UFBoot2: Improving the ultrafast bootstrap approximation. *Molecular Biology and Evolution* 35: 518–522.
- Horn S, Pabón-Mora N, Theuß VS, Busch A, Zachgo S. 2015. Analysis of the *CYC1/TB1* class of TCP transcription factors in basal angiosperms and magnoliids. *The Plant Journal* 81: 559–571.
- Howarth DG, Donoghue MJ. 2006. Phylogenetic analysis of the “ECE” (*CYC1/TB1*) clade reveals duplications predating the core eudicots. *Proceedings of the National Academy of Sciences, USA* 103: 9101–9106.
- Howarth DG, Martins T, Chimney E, Donoghue MJ. 2011. Diversification of *CYCLOIDEA* expression in the evolution of bilateral flower symmetry in Caprifoliaceae and *Lonicera* (Dipsacales). *Annals of Botany* 107: 1521–1532.
- Kalyanamoorthy S, Minh BQ, Wong TKF, Von Haeseler A, Jermiin LS. 2017. ModelFinder: fast model selection for accurate phylogenetic estimates. *Nature Methods* 14: 587–589.
- Katoh K, Misawa K, Kuma K, Miyata T. 2002. MAFFT: a novel method for rapid multiple sequence alignment based on fast Fourier transform. *Nucleic Acids Research* 30: 3059–3066.
- Kosugi S, Ohashi Y. 2002. DNA binding and dimerization specificity and potential targets for the TCP protein family. *The Plant Journal* 30: 337–348.
- Koyama T, Furutani M, Tasaka M, Ohme-Takagi M. 2007. TCP transcription factors control the morphology of shoot lateral organs via negative regulation of the expression of boundary-specific genes in *Arabidopsis*. *Plant Cell* 19: 473–484.
- Leppik EE. 1972. Origin and evolution of bilateral symmetry in flowers. *Evolutionary Biology* 5: 49–85.
- Li C, Potuschak T, Colón-Carmona A, Gutiérrez RA, Doerner P. 2005. Arabidopsis TCP20 links regulation of growth and cell division control pathways. *Proceedings of the National Academy of Sciences, USA* 102: 12978–12983.
- Li M, Zhang D, Gao Q, Luo Y, Zhang H, Ma B, Chen C, Whibley A, Zhang Y, Cao Y *et al.* 2019. Genome structure and evolution of *Antirrhinum majus* L. *Nature Plants* 5: 174–183.
- Li S. 2015. The *Arabidopsis thaliana* TCP transcription factors: a broadening horizon beyond development. *Plant Signaling and Behavior* 10: e1044192.
- Li S, Gutsche N, Zachgo S. 2011. The ROXY1 C-Terminal L**LL motif is essential for the interaction with TGA transcription factors. *Plant Physiology* 157: 2056–2068.
- Lin YF, Chen YY, Hsiao YY, Shen CY, Hsu JL, Yeh CM *et al.* 2016. Genome-wide identification and characterization of TCP genes involved in ovule development of *Phalaenopsis equestris*. *Journal of Experimental Botany* 67: 5051–5066.
- Luo D, Carpenter R, Copey L, Vincent C, Clark J, Coen E. 1999. Control of organ asymmetry in flowers of *Antirrhinum*. *Cell* 99: 367–376.
- Luo D, Carpenter R, Vincent C, Copey L, Coen E. 1996. Origin of floral asymmetry in *Antirrhinum*. *Nature* 383: 794–799.
- Madrigal Y, Alzate JF, Pabón-Mora N. 2017. Evolution and expression patterns of TCP genes in Asparagales. *Frontiers in Plant Science* 8: 9.
- Martín-Trillo M, Cubas P. 2010. TCP genes: a family snapshot ten years later. *Trends in Plant Science* 15: 31–39.

- Miller MA, Pfeiffer W, Schwartz T. 2010. *Creating the CIPRES Science Gateway for inference of large phylogenetic trees*. [WWW document] URL <http://www.phylo.org> [accessed 5 June 2020].
- Mondragón-Palomino M, Trontin C. 2011. High time for a roll call: gene duplication and phylogenetic relationships of TCP-like genes in monocots. *Annals of Botany* 107: 1533–1544.
- Nath U, Crawford BC, Carpenter R, Coen E. 2003. Genetic control of surface curvature. *Science* 299: 1404–1407.
- Navaud O, Dabos P, Carnus E, Tremouyague D, Hervé C. 2007. TCP transcription factors predate the emergence of land plants. *Journal of Molecular Evolution* 65: 23–33.
- Nguyen LT, Schmidt HA, Minh BQ. 2015. IQ-TREE: a fast and effective stochastic algorithm for estimating maximum-likelihood phylogenies. *Molecular Biology and Evolution* 32: 268–274.
- Pabón-Mora N, Suárez-Baron H, Ambrose BA, González F. 2015. Flower development and perianth identity candidate genes in the basal angiosperm *Aristolochia fimbriata* (Piperaceae: Aristolochiaceae). *Frontiers in Plant Science* 6: 1095.
- Palatnik JF, Allen E, Wu X, Schommer C, Schwab R, Carrington JC, Weigel D. 2003. Control of leaf morphogenesis by micro-RNAs. *Nature* 425: 257–263.
- Parapunova V, Busscher M, Busscher-Lange J, Lammers M, Karlova R, Bovy AG *et al.* 2014. Identification, cloning and characterization of the tomato TCP transcription factor family. *BMC Plant Biology* 14: 157.
- Pérez-Mesa P, Ortiz-Ramírez CI, González F, Ferrándiz C, Pabón-Mora N. 2020. Expression of gynoceium patterning transcription factors in *Aristolochia fimbriata* (Aristolochiaceae) and their contribution to gynostemium development. *EvoDevo* 11: 4.
- Preston JC, Hileman LC. 2012. Parallel evolution of TCP and B-class genes in Commelinaceae flower bilateral symmetry. *EvoDevo* 3: 6.
- Preston JC, Kost MA, Hileman LC. 2009. Conservation and diversification of the symmetry developmental program among close relatives of snapdragon with divergent floral morphologies. *New Phytologist* 182: 751–762.
- Rambaut A. 2014. *FigTree: tree figure drawing tool*. [WWW document] URL <http://tree.bio.ed.ac.uk/software/figtree/>.
- Rudall PJ, Bateman RM. 2004. Evolution of zygomorphy in monocot flowers: iterative patterns and developmental constraints. *New Phytologist* 162: 25–44.
- Sargent RD. 2004. Floral symmetry affects speciation rates in angiosperms. *Proceedings of the Royal Society of London* 271: 603–608.
- Suárez-Baron H, Alzate JF, González F, Ambrose BA, Pabón-Mora N. 2019. Genetic mechanisms underlying perianth epidermal elaboration of *Aristolochia ringens* Vahl (Aristolochiaceae). *Flora* 253: 56–66.
- Suárez-Baron H, Pérez-Mesa P, Ambrose BA, González F, Pabón-Mora N. 2016. Deep into the *Aristolochia* flower: expression of C, D and E class genes in *Aristolochia fimbriata* (Aristolochiaceae). *Journal of Experimental Zoology Part B: Molecular and Developmental Evolution* 328: 55–71.
- Viola I, Uberti-Manassero N, Ripoll R, González D. 2011. The Arabidopsis class I TCP transcription factor AtTCP11 is a developmental regulator with distinct DNA-binding properties due to the presence of a threonine residue at position 15 of the TCP domain. *Biochemical Journal* 435: 143–155.
- Wang J, Wang Y, Luo D. 2010. LjCYC genes constitute floral dorsoventral asymmetry in *Lotus japonicus*. *Journal of Integrative Plant Biology* 52: 959–970.
- Yuan Z, Gao S, Xue DW, Luo D, Li LT, Ding SY, Yao X, Wilson ZA, Qian Q, Zhang D. 2009. RETARDED PALEA1 controls palea development and floral zygomorphy in rice. *Plant Physiology* 149: 235–244.
- Zhang W, Kramer EM, Davis CC. 2010. Floral symmetry genes and the origin and maintenance of zygomorphy in a plant–pollinator mutualism. *Proceedings of the National Academy of Sciences, USA* 107: 6388–6393.
- Zhang W, Steinmann VW, Nikolov L, Kramer EM, Davis CC. 2013. Divergent genetic mechanisms underlie reversals to radial floral symmetry from diverse zygomorphic flowered ancestors. *Frontiers in Plant Science* 4: 302.

Supporting Information

Additional Supporting Information may be found online in the Supporting Information section at the end of the article.

Fig. S1 Expanded ML phylogenetic analysis of the class II *TCP* genes in angiosperms.

Fig. S2 MEME analysis and mapping of domains and motifs found in class II *TCP* proteins.

Fig. S3 Sequences of domains and motifs found by the MEME analysis.

Fig. S4 RT-PCR expression analysis of the class II *TCP* genes in the flowering apices and the dissected perianth dorsal and ventral portions of *Aristolochia fimbriata*.

Fig. S5 *In situ* hybridization of *AfimCYC* showing expression in the accessory buds.

Fig. S6 Prosite scan on the VEWLI and the VDWLI motifs of CIN1 and CIN3 proteins.

Table S1 Plant vouchers and transcriptome statistics obtained for each of the members of the perianth-bearing Piperaceae.

Table S2 Primers used in this study.

Please note: Wiley Blackwell are not responsible for the content or functionality of any Supporting Information supplied by the authors. Any queries (other than missing material) should be directed to the *New Phytologist* Central Office.